Translated from *Uspekhi Khimii*, **46**, 2240 - 2263 (1977) U.D.C. 546.23-126;535.215

Photoelectric Phenomena in Polymeric Selenium Structures

Yu.A.Cherkasov and N.B.Zakharova

In order to clarify the phenomenon of non-photoactive absorption in molecular solids we have analysed the relationship between the spectra of photoelectric phenomena in selenium and the molecular (and supermolecular) structures of selenium. Non-photoactive absorption is shown to arise from the photo-generation of charge carriers through the state of bound electron-hole pairs (excitons), which is structure-sensitive and dependent on quantum energy, temperature, and applied field intensity. 109 references.

CONTENTS

I. Introduction (the problem of non-photoactive absorption in molecular solids) 1188
II. Crystal structures of selenium 1188
III. Amorphous and amorphous-crystalline selenium structures (microcrystalline phase and phase boundary) 1190
IV. Amorphous analogues of selenium crystal structures 1194
V. Photosensitivity and the structural sensitisation of the photo-effect 1196

I. INTRODUCTION (THE PROBLEM OF NON-PHOTOACTIVE ABSORPTION IN MOLECULAR SOLIDS)

Photoelectric phenomena are among the most important manifestations of the interaction between light and matter, underlying many biological processes (photosynthesis, colour vision) as well as the fixation of optical images (photographic processes). Recent systematic studies of the absolute quantum yield of photoelectric phenomena in molecular (polymeric) photoconductors have led to the hypothesis of non-photoactive edge absorption in these materials, in contrast to the classical crystalline semiconductors such as germanium and silicon. Non-photoactive absorption, extending partly into the depth of the absorption band, has been observed in molecular photoconductors of various classes, including organic (anthracene) and inorganic (selenium) crystalline photoconductors, amorphous inorganic photoconductors (amorphous selenium structures and selenium structures with tellurium, arsenic, and germanium hetero-atoms), organic poly-conjugated polymeric photoconductors (polyacetylenes), organic saturated polymeric photoconductors (vinyl polymers), and also dye-sensitised organic polymers[1-5]. The basic factor which determines the appearance of non-photoactive absorption in these photoconductors is the photo-generation of charge carriers through the state of a bound hole–electron pair (exciton), depending on the quantum energy, the temperature, and the strength of the applied electric field. The effect is found to be structure-sensitive: some selenium structures (both crystalline and amorphous) do not show non-photoactive absorption over a wide range of quantum energy, giving an internal photo-effect with a very high quantum yield (approaching 100%) over the whole visible region of the spectrum.

In this review we shall analyse the relationship between the molecular (and supermolecular) selenium structures and the spectra of the photoelectric phenomena in selenium. Amorphous, amorphous–crystalline, and crystalline selenium structures will be considered, with special emphasis on the photoelectric phenomena in the presence of external electric fields: photoconductivity (electrophotographic sensitivity) in strong fields, which collect all the light-generated carriers and allow us to measure one of the most important characteristics of the interaction of light with matter (the quantum yield of the internal photo-effect, equal to the number of hole–electron pairs created by each quantum of light absorbed), and photoconductivity in weak electric fields, in particular at very high frequencies, which allows us to minimise the influence of contacts and to study photoconduction with very small "displacements" of the charge carriers. We shall also discuss photoelectric phenomena in the absence of applied electric fields, and in particular the diffusion of photocarriers along a concentration gradient (capacitive photo-e.m.f. and contact potential difference).

The modern view of the structure of selenium is of an inorganic polymer which can easily change its molecular and supermolecular structure[6]. A clear understanding of the correlation between the structure and the properties of such an inorganic polymer, which is highly photosensitive over a wide spectral region, should help us to formulate methods of controlling the physical properties of polymers in general, and in particular it should suggest ways of improving the photosensitivity of organic polymers.

II. CRYSTAL STRUCTURES OF SELENIUM

1. Structure of the Molecule and Allotropic Forms

Selenium forms complex molecules easily altered under the influence of various factors. This feature of selenium is responsible for the existence of several allotropic forms of selenium in the solid state, able to coexist over a wide range of temperature[7]. The state of the outer electrons in an isolated selenium atom corresponds to the $4s^2 4p^4$ configuration. Of the six outer electrons, two (paired) are in the s-state, and two (paired) in the p-state, and do not take part in bond formation. The bond between atoms is created by the two unpaired electrons. The electron clouds of the unpaired p-electrons of each atom overlap the p-clouds of the neighbouring atoms to give filled p-orbitals. The bond angle (105.5°) causes the atoms to adopt a helix configuration in the molecular chain, or alternatively to form eight-membered rings. We note that selenium can have a valence of 4 or 6 as a result of the transition of two or four unpaired electrons from p (or s and p) orbitals into a d-orbital[8]. The interatomic bonding within

the molecule is strong and covalent, though the nature of the intermolecular bonds is still controversial. Some workers[9,10] argue, in view of the low melting point and of the easy cleavage of the crystal along planes parallel to the molecular chains, that the intermolecular forces must be of the Van der Waals type. Others[11] stress that the distance between chains in selenium is too short for Van der Waals interactions and that the coordination number is greater than the maximum possible number of p-bonds, and conclude that rotary resonance of the chemical bonds is present in selenium crystals. Bond hybridisation is postulated, extending over four atoms of the second coordination sphere of different molecular chains. Hybrid orbitals have a greater bond energy than non-hybridised orbitals, and therefore their stability is higher[12]. Furthermore we expect intermolecular energy barriers to be lowered by the presence of hybridised bonds[12].

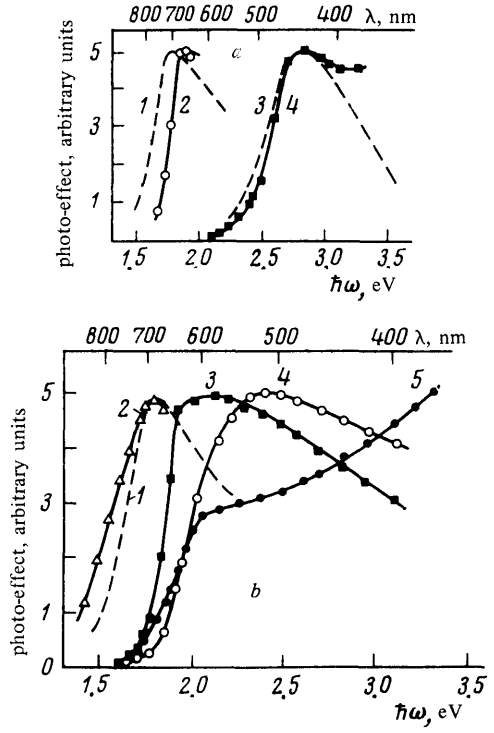


Figure 1. Photo-effect spectra of the crystalline selenium structures and of the corresponding amorphous analogues: (*a*) *1*) trigonal selenium, *2*) its amorphous analogue, *3*) monoclinic selenium, *4*) its amorphous analogue; *1*) and *3*) d.c. photoconductivity, *2*) and *4*) electrophotographic sensitivity[23]; (*b*) trigonal selenium; *1*) d.c. photoconductivity[24], *2*) and *3*) electrophotographic sensitivity of a polycrystalline sample[1] and of microcrystals dispersed in an organic matrix[23] respectively, *4*) photo-e.m.f., *5*) contact potential difference.

The most stable crystalline form of selenium is the trigonal modification. The monoclinic (α and β) and the cubic (α and β) modifications, with different elementary cells in different space groups, are also true crystalline phases[7]. The structural features of the crystalline forms are largely determined by the molecular structure of selenium[13]. The basic structural element of trigonal selenium is a polymeric helical molecular chain with an interatomic distance of 2.32 Å and a bond angle of 105.5°. A parallel orientation of such chains, with an axial separation of 3.48 Å, creates a hexagonal lattice with parameters $a = 4.35$ and $c = 4.94$ Å.[14] Another crystal form (α and β monoclinic selenium) is formed from eight-membered, puckered selenium molecules (closed rings in the α modification, open rings in the β modification) with an interatomic distance of 2.3 Å,[15] a spacing of 2.9 Å between rings, and lattice parameters $a = 9.1$, $b = 9.1$, $c = 11.6$ Å, $\varphi = 90°16'$ for α-monoclinic selenium[16-18]. Both modifications are molecular crystals. For the cubic modifications[19,20] we have $a = 2.97$ Å (for the α-cubic lattice) and a bond length of 2.97 Å.

2. Photoelectric Phenomena

The photoelectric properties of crystalline selenium have been studied by various methods, including photoconductivity in strong electric fields (electrophotographic (EP) sensitivity)[21], photoconductivity at ultra-high (10^{10} Hz) frequency[22], capacitive photo-e.m.f., influence of light on the contact potential difference, etc.[23-26]. Spectral curves for the photo-effects observed by the above methods in monoclinic and trigonal selenium are shown in Fig. 1. The EP sensitivity spectrum (curves *2* and *3* of Fig. 1*b*) extends over the whole visible region of the spectrum up to 800 nm. Its long-wavelength edge is close to the edge of the photoconductivity spectrum of polycrystalline layers of trigonal selenium (curve *1* of Fig. 1*b*). We should note that the EP sensitivity (curve *3* of Fig. 1*b*) is discussed in terms of a model consisting of a dispersion of trigonal selenium microcrystals (of micrometre dimensions) in an organic matrix based on styrene copolymers[21]. Single crystals of trigonal selenium have zero EP sensitivity because their resistance is too low to give an acceptably long relaxation time. Transverse current can be obtained in these heterogeneous layers in fields of 10^4–(2×10^5) V cm^{-1} if the gaps between crystallites are not too great (a few nanometers).

The photo-e.m.f. and contact potential difference spectra (curves *4* and *5* of Fig. 1*b*) are displaced towards shorter wavelengths, as are the corresponding spectra of organic photoconductors[27]. On the other hand, the EP sensitivity curve of polycrystalline trigonal selenium (curve *2* of Fig. 1*b*) has a maximum at 700 nm, characteristic of the single crystals and coinciding with the photoconductivity maximum of the individual microcrystals measured at a frequency of 10^{10} Hz.[22] In these measurements the red edge of the photoconductivity lies at longer wavelengths than the red edge of other photoelectric effects. By comparing the EP sensitivity and the photoconductivity curves we conclude that the low EP sensitivity in the long-wavelength part of the spectrum arises from the specific structure of the heterogeneous (amorphous–crystalline) system, resulting in a particular field distribution. Because of the short Debye screening length, the electric field penetrates into the selenium microcrystals to a depth of only 0.1 μm, and only the surface regions of the crystals are able to contribute to the EP sensitivity of the system. Generation of hole–electrons pairs in the depth of the crystals cannot contribute to the EP sensitivity if the applied electric field is excluded from these regions. The range of quantum energy in which the EP sensitivity is

found to fall corresponds to a decrease in the absorption coefficient from 10^5 cm^{-1} (for 2.1 eV) to 10^4 cm^{-1} (for 1.8 eV). Exciton effects associated with non-photoactive absorption cannot be excluded, but while the results do not contradict this interpretation they do not positively confirm it.

In contrast to trigonal selenium, with the monoclinic form of selenium the spectra of the photoelectric effects are shifted (curves *3* and *4* of Fig. 1*a*) towards the centre of the absorption band (curve *7* of Fig. 5*a*).

The crystal structure of selenium consisting of long helical molecules (trigonal selenium) differs from that consisting of closed eight-membered rings (monoclinic selenium) in having an internal photo-effect with a quantum yield close to 100% over a wide region of the spectrum (see curve *1* of Fig. 6*a*).[28] This is the only known example of a molecular crystal in which the yield of the internal photo-effect is maximal over a wide spectral range.

III. AMORPHOUS AND AMORPHOUS–CRYSTALLINE SELENIUM STRUCTURES (MICROCRYSTALLINE PHASE AND PHASE BOUNDARY)

1. Amorphous–Crystalline Structures

The essential feature of the structure of matter in an amorphous state is the absence of long-range order in the arrangement of its atoms or molecules. The term order (long-range or short-range) denotes the correlation in the mutual disposition of atoms or molecules in the solid: a correlation at a distance of the same order as the mean interatomic spacing is termed short-range order, whereas a correlation without limit as to distance is termed long-range order. Amorphous and amorphous–crystalline selenium structures can be prepared both from the gas phase (by thermal evaporation in a vacuum) and from the liquid phase (by quenching)[6,29].

a) Molecular composition of the melt. As we have already pointed out, the crystal lattices of all the known modifications of selenium are built up from different structural units. Hence these structural units must be present as equilibrium forms[7] when selenium is crystallised (from the vapour, the liquid, or the amorphous state) to give one or other of the crystalline modifications of the element. However we do not clearly understand the conditions of formation of these structural units, their stability, or their mutual interconversion. The main difficulty is the presence of molecules of different structure and size in selenium samples at any temperature below the melting point (220°C). Several workers have found that the liquid phase consists of closed rings and molecular chains of different size, whereas selenium vapour (up to 1000°C) consists of a mixture of molecules (containing eight, six, four, or two atoms) and single atoms. Liquid selenium retains all the attributes of a molecular liquid down to 200°C,[29-32] and is reported[33] to be associated.

Existing information on the form and relative amount of the different molecules in liquid selenium is contradictory. Some workers[34] state that liquid selenium consists of helical molecular chains, while others[35,36] suggest that parallel orientation of the chains persists up to 300°C. X-ray diffraction studies[32,35] have shown that six- and eight-membered rings are present in liquid selenium. More recent work[37,38] has led to the suggestion that eight-membered rings are in equilibrium with polymeric chains in liquid selenium. The formation of long polymeric chains begins at a critical temperature (83°C) well below the melting point of selenium, the rate of formation increasing with temperature. It is reported[38,39] that at the melting point the chains contain at least 10^2–10^4 atoms of selenium. Other workers[40] find that at 220°C the mean chain length in pure selenium is 2×10^5 atoms. The high-polymer nature of liquid selenium has been demonstrated by viscosity measurements[41], according to which the polymeric chains contain up to 500 atoms at temperatures up to 220°C.

Contradictory information has been published also on the temperature dependence of the melt composition. Measurements of magnetic susceptibility[35,36,42] suggest that the dissociation of the selenium molecules is insignificant in the region of 230–650°C. On the other hand, substantial structural changes in liquid selenium have been observed[33,43] over the range 300–320°C, but the nature of these changes is unknown. Thus practically all the structural units of the crystalline forms are present in liquid selenium, including[32,35] small regions of normal hexagonal lattice. Selenium samples prepared from the liquid or the vapour phase are believed to include equilibrium structural units of the different crystalline modifications, which can subsequently undergo crystallisation or formation of an amorphous state[7].

In spite of the apparent simplicity of the vacuum evaporation method, the deposition of thin films of amorphous selenium gives poorly reproducible results, and the relationship between the deposition conditions and the structure and physical properties of the films is still not clear. A great deal of information has been published on metallic films[44,45], but the deposition of a material like selenium in the form of thin films differs radically from the deposition of metal films, because the beam of evaporating material is molecular in the former case and atomic in the latter[45]. The structure of films resulting from the condensation of vapour produced by vacuum evaporation depends on the physicochemical properties of the solid source and on the evaporation conditions: residual pressure in the vacuum chamber, rate of deposition, temperature and structure of the substrate, etc.[44] The molecular composition of the vapour is by no means the least important condition[46].

b) Effect of the molecular composition of the vapour on film structure. The molecular structure of selenium vapour depends on its temperature. Above 1500°C selenium molecules dissociate into atoms: the selenium–selenium bond energy of diatomic molecules, determined from spectroscopic data and from the heat of dissociation[6], is 2.9 ± 0.2 eV. When the temperature is lowered to 1000°C the vapour phase includes molecules of all degrees of complexity between monatomic and eight-atomic, the relative amounts depending on temperature. Molecular complexes and quasi-crystalline formations apparently exist in the vapour phase at not too high temperatures. The evaporation of selenium as molecular complexes, which persist in the vapour phase up to 680°C, enables the molecular and super-molecular forms present in the source material to be transported to the condensing layer[43,47]. Nesmeyanov[48] critically reviewed published work on the temperature dependence of the pressure and composition of selenium vapour, and concluded that insufficient information is available on vapour composition at temperatures close to the melting point. Two papers[49,50] are selected[48] as the most reliable. One of these[49] treats the evaporation of selenium as the formation of an equilibrium mixture of diatomic and six-atomic molecules, the

proportion of diatomic molecules increasing with temperature from 12% (at 185°C) to 25% (at 684°C, the boiling point of selenium). According to the second paper[50] selenium vapour at 550–900°C contains tetra-atomic and eight-atomic molecules in addition to diatomic and six-atomic, the relative amount of each species being a function of temperature. Molecules containing eight atoms have been shown to be present in small amounts at temperatures below 500°C by a vapour density method, and the formation of a small amount of atomic selenium at temperatures near 1000°C has been confirmed by the same method[51,52]. Electron-diffraction studies[53] have shown that selenium vapour at ~ 450°C consists mainly of six-membered molecular rings in the "chair" configuration, with a smaller number of diatomic molecules.

Thus at the evaporation temperatures (300–500°C) normally used for the deposition of thin films of amorphous selenium the vapour consists mainly of six-atomic molecules. Diatomic molecules are also present, at lower concentration. The structural, electrical, and photoelectric properties of amorphous selenium layers are reported[46] to be very sensitive to the temperature of the selenium vapour (in the range 200–900°C) from which the layers are deposited. The phenomenon is ascribed partly to the role of the thermal velocity of the molecules, and partly to the degree of dissociation of the molecules. Unfortunately these two factors could not be separated in the experiments described.

c) Effect of residual gas pressure on film structure. Another important parameter influencing the structure of amorphous selenium layers is the pressure of residual gases in the chamber[54]. Thus, with a residual air pressure $> 6 \times 10^{-2}$ mmHg we obtain sooty, rough layers of low average density with a fibrous surface structure. Other gases (e.g. oxygen and argon) have a similar effect on the macro-structure of the layer when present at pressures $> 6 \times 10^{-2}$ mmHg. At pressures $< 2 \times 10^{-2}$ mmHg, where the mean free path of the evaporating molecules becomes comparable to the distance between the evaporator and the target, the residual gas molecules cease to affect the condensation of selenium, and dense layers with a mirror-smooth surface are obtained by vacuum evaporation. However the properties of these layers are still strongly dependent on the nature of the residual gas.

It has been suggested[54] that molecules or atoms of the residual gas can be incorporated in the condensing layers, thus influencing their microstructure or acting as electrically active impurities (which influence the electrical and photoelectric properties of the layers). Unfortunately no systematic study of the effect of residual gas pressure on the microstructure of amorphous selenium layers appears to have been reported. Electron-microscopic measurements[55] failed to show any structural difference between layers deposited at different residual gas pressures in the range from 10^{-3} to 10^{-6} mmHg. Furthermore, if the residual gas in the chamber has a high affinity for selenium we can expect compound formation at high substrate temperatures and high background pressures. Hence the preparation of dense and pure films of amorphous selenium should only be attempted in a vacuum of 10^{-5} mmHg or better.

d) Effect of rate of deposition on film structure. The rates of condensation used in the preparation of amorphous selenium films are quite high and usually in excess of 1 μm min^{-1} (i.e. about 100 atomic layers per second). These high rates of condensation lead to the evolution of substantial amounts of latent heat, and because of the low thermal conductivity of amorphous selenium ($\sim 3 \times 10^{-4}$ cal cm^{-1} s^{-1} K^{-1}) this effect gives the molecules of condensate a high surface mobility and assists structural rearrangements within the layer[46]. However experiments[46] at rates of condensation between 0.5 and 2.5 μm min^{-1} failed to reveal any difference in the electrical and photoelectric properties of amorphous selenium films. This suggests that the structure of amorphous selenium becomes insensitive to deposition rate at these high rates of deposition.

e) Effect of substrate temperature on the structure. The structure of the selenium layers is affected most markedly by the temperature of the substrate during deposition[8,15,56–62] and by the subsequent annealing conditions[8,37,38,63–65]. The effect of substrate temperature (in the range 0–100°C) on the structure of the selenium layers has been studied[57] by electron microscopy and by X-ray and electron diffraction. Layers prepared at substrate temperatures between 0 and 10°C had a pale grey surface, changing to red when the substrate temperature was raised to 35–40°C. The surface of layers prepared at low substrate temperatures is covered with hillocks. At higher substrate temperatures the layers develop a dark red colour and a mirror-smooth surface. X-ray and electron diffraction studies[57] and optical studies in polarised light[8,15,57] have confirmed that the structure of these layers is amorphous immediately after preparation. The proportion of crystalline phase in samples prepared at a substrate temperature of 90–100°C is only 7–8%.

2. Amorphous Forms of Selenium

Nabitovich and coworkers point out[57] that layers prepared at low (20–30°C) and intermediate (50–60°C) substrate temperatures have different amorphous structures: both the height and the width of the diffraction peaks are different in the X-ray and the electron diffraction patterns. The presence of different amorphous structures in selenium has been reported also by other workers[29,32,58,61,63]. Electron diffraction studies of the structure of thin layers of amorphous selenium deposited on cellulose nitrate substrates at 20°C have shown[63] the presence of two forms of amorphous selenium, characterised by different coordination numbers and different radii of the coordination sphere. The first is formed at substrate temperatures around 20°C, the second becomes predominant at substrate temperatures of 60–70°C. A gradual transition from one form to the other can be achieved at intermediate temperatures without going through a crystalline form. At 30–40°C the deposited layer is a mixture of approximately equal amounts of the two forms. Nabitovich and coworkers[15,16] evaluated the short-range order parameter in different forms of amorphous selenium and determined their molecular structure. Condensation on substrates at 20°C produces the first form of amorphous selenium, consisting mainly of eight-membered molecular rings; the second form, consisting mainly of long molecular chains of selenium, is obtained at substrate temperatures of 50–55°C. The crystallisation processes of these two forms of amorphous selenium are also quite different[15].

Some earlier workers[29,58] also reported two different forms of amorphous selenium, detected by X-ray diffraction, but differing in structure from those reported in Refs. 15 and 63. Thus selenium deposited on substrates

cooled to −180°C was found[29] to have an amorphous "packet" structure consisting of six-membered molecular rings. This report was later confirmed[56]. The authors[29] were led to the hypothesis of a packet structure of six-membered rings by an analysis of the diffraction patterns of films obtained under different condensation conditions (in particular, the molecular composition of the vapour and the substrate temperature during deposition). The second form of amorphous selenium is observed[58] when selenium is evaporated on to substrates at 20°C, and consists mainly of molecular chains similar in structure to those of trigonal selenium. Furthermore, selenium samples prepared at room temperature often contain micro-crystals of trigonal selenium[29,58]. The presence of molecular chains in the layers was confirmed by neutron diffraction and X-ray diffraction studies of amorphous selenium structures[67].

In contrast to these findings, Richter and Herre[29] report that selenium layers formed at 20°C consist of a mixed phase of molecular chains, six-membered rings, and elements of the normal hexagonal selenium lattice. Richter later showed by X-ray structural analysis[68] that selenium layers are predominantly in one of three amorphous forms, depending on the method of preparation: all three forms have the chain structure characteristic of trigonal selenium but the interatomic distance within the chain is different in the three cases. In an earlier investigation[69] the X-ray data obtained from similar samples had been interpreted as evidence for an amorphous selenium structure composed of eight-membered rings (characteristic of monoclinic selenium).

3. Crystallisation of Amorphous Selenium

The vapour deposition of selenium at substrate temperatures above 60°C invariably produces layers containing some crystalline phase[8,59,70]: on raising the temperature of the substrate the concentration of the crystalline phase increases[8,59], and at substrate temperature of 80–90°C a continuous layer of trigonal selenium is formed on the substrate surface[8,60,62]. We should note that amorphous selenium crystallises spontaneously to an appreciable extent even at room temperature[8,59,70,71]. Crystallisation is fastest in amorphous layers prepared on substrates at temperatures below 20°C: such layers are fully crystalline after a few months.

It is well established that the crystallisation of amorphous selenium occurs in two steps: nucleation and crystal growth. The optimum nucleation temperature is 130°C, whereas the best temperature for crystal growth is 210°C. According to Krebs[30,41] crystallisation begins at specific sites in the amorphous selenium, where small ordered regions of parallel chains (micelles) are formed. On raising the temperature the micelles can grow at the expense of the amorphous selenium. On the other hand, selenium often forms spherulites[30,41]—a special type of rounded, textured polycrystalline formation growing from a single centre, often encountered in the crystallisation of polymers. The temperature range of spherulitic crystallisation for amorphous selenium is 70–150°C.

The rate of crystallisation of selenium is strongly influenced by the annealing schedule, by the purity of the starting material, and by some external conditions. Increase of temperature produces a sharp increase in the rate of crystallisation, the time for complete crystallisation varying from several hours at 70°C to 2–3 min at 217°C. Impurities such as thallium, antimony, indium, alkali metals, oxygen, and halogens catalyse the conversion of amorphous into trigonal selenium.

The action of light, electrons, positive ions, γ-rays, electric fields, and various organic or inorganic solvents also favours the conversion of amorphous selenium into a thermodynamically more stable crystalline state[6].

Selenium layers prepared under uncontrolled or special conditions may contain all the known amorphous and crystalline phases. Thus layers prepared by the sublimation method[72–76] are evaporated on to the substrate from another surface held at 185°C, the substrate temperature is then raised to 83°C and the layer is held at this temperature for approximately 15 min to stabilise the structure. Films prepared in this way contain a layer of trigonal selenium (adjacent to the surface of the substrate), and a layer of glassy selenium consisting of the amorphous forms. It has been shown[62,77,78] that vacuum evaporation of selenium on a substrate at ~ 85°C produces small islands of crystalline selenium[77] which merge into a continuous sublayer of trigonal selenium at a higher substrate temperature (98°C). The thickness of the crystalline sublayer depends on the temperature of the substrate[78,81]: ~ 0.1 μm at 70°C and 0.8 μm at 90°C. At a substrate temperature of 70–80°C the crystalline layer is fairly smooth, but at higher temperatures we observe dendritic growth to a diameter of 1 μm (at 90°C) and to a depth of 1–2 μm into the layer. At 70–80°C we find, between the trigonal and the amorphous layer, a layer 0.1–0.4 μm thick consisting of a mixture of the monoclinic and the trigonal modification, which is gradually converted into the trigonal modification at room temperature.[80] At 50–60°C the continuous crystalline layer is not formed, but separate crystalline inclusions up to several hundred μm^2 in area are produced. Crystallisation can be retarded by depositing a sublayer of arsenic triselenide 0.2–0.5 μm thick[79]. Evidently, the same result is obtained using a layer of cellulose nitrate[82,83], which stabilises the properties of layers prepared at 65°C.

Following Nabitovich[7] we can summarise our understanding of the selenium structures as follows. It is now well established that the structure of selenium films is determined first and foremost by the technological conditions used in their preparation. When the films are prepared by vacuum condensation of a molecular vapour on an isotropic substrate the structure is determined by the temperature of the melt, the condensation time, the substrate temperature, and the post-deposition annealing conditions. Immediately after deposition these layers can be in three states: crystalline, supercooled, or amorphous. Condensation of selenium on a substrate at 97–100°C invariably yields crystalline layers, irrespective of the rate of condensation. Selenium layers condensed on substrates at 60–100°C and rapidly cooled to room temperature are always in a supercooled metastable state.

4. Photo-electric Phenomena in Amorphous Selenium Structures

Amorphous selenium structures show photosensitivity in the region of $\lambda < 600$ nm (Fig. 2). The photosensitivity spectrum in the visible region has two more or less sharply defined maxima[1] at 370 and 470 nm (curves *1* and *2* of Fig. 2*b*). The photosensitivity increases as the wave length decreases to 140 nm (Fig. 2*a*). This increase arises from the multiplication of the photo-generated

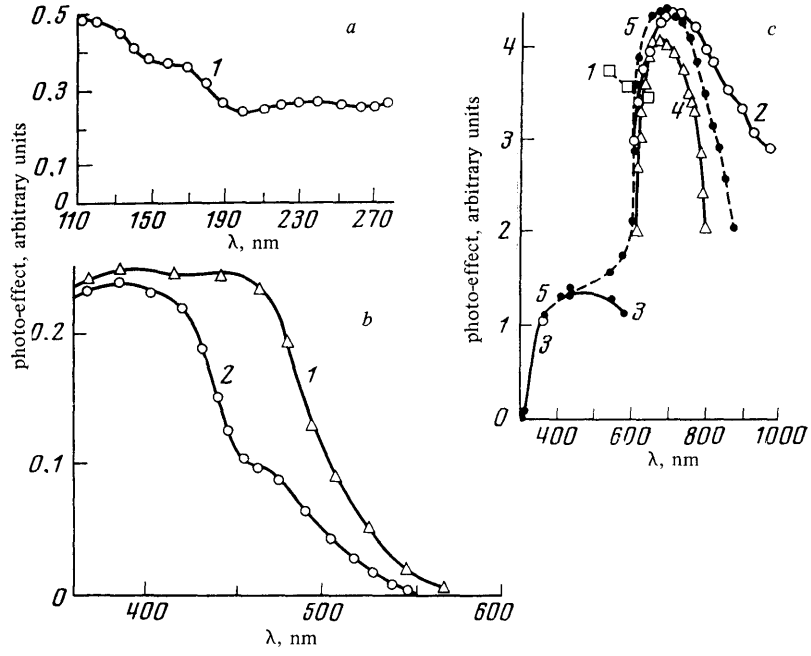


Figure 2. Photo-effect spectra of the amorphous and amorphous–crystalline selenium structures: (*a*) and (*b*) d.c. photoconductivity (electrophotographic sensitivity) of amorphous selenium[91]; (*b*) *1*) layer prepared at 300 K, *2*) 120 K; (*c*) photoconductivity at 10^{10} Hz[22]: *1*) amorphous selenium (second amorphous form), *2*) amorphous selenium containing 30% of trigonal selenium, steady illumination, *3*)–*5*) modulated illumination, amorphous selenium with different amounts of crystalline phase (*3*) 1–2%, *4*) > 10%, *5*) 30%). The curves for steady (*2*) and modulated (*5*) illumination are normalised to the same peak value; a logarithmic scale is used for the photo-effect.

current carriers at photon energies greater than the forbidden energy gap of selenium in the absence of concentration-dependent recombination. Lowering the substrate temperature during deposition to −150°C lowers the photosensitivity in the spectral region above 400 nm (curve *2* of Fig. 2*b*). Conversely, heat treatment of the amorphous selenium layer, leading to the appearance of a crystalline phase, increases the photosensitivity in the long-wavelength region of the spectrum (Fig. 2*c*). Heat treatment of the layers in air at 60°C for 24 h extends the region of photosensitivity to 880 nm.

The sensitivity spectra of the amorphous and the crystalline phase in heterogeneous selenium layers have been studied by photoconductivity measurements at ultra-high frequencies[22] with steady illumination[85] and with light modulated at 200 Hz.[86] These measurements make clear the relationship between the bulk photoconducting properties and the molecular and supermolecular structure of the selenium sample under conditions which minimise the effect of contacts and allow the photoconductivity to be studied with small "displacements" of the carriers. The basic characteristics of the photoconductivity, i.e. its magnitude, spectral distribution, and temperature dependence, are a function of the amount of crystalline phase in the amorphous selenium. Thus, with 1–2% of crystalline phase photoconductivity (with positive photo-carriers) is observed in the region of 300–600 nm (curve *3* of Fig. 2*c*). The photoconductivity limits of the layers are different for a frequency of 10^{10} Hz ($\Delta\sigma_{\sim}$) and for direct current ($\Delta\sigma_{=}$). With direct current $\lambda_{\frac{1}{2}} \simeq 500$ nm,[25,87] i.e. well within the optical absorption band (absorption edge ~ 600 nm). The $\Delta\sigma_{\sim}$ limit, as shown in curve *5* of Fig. 2*c*, occurs at the wavelength $\lambda_{\frac{1}{2}} \simeq 750$ nm, i.e. beyond the absorption edge. Increasing the amount of crystalline phase to 10–30% produces a large (approximately 1000-fold) increase of $\Delta\sigma_{\sim}$ in the red region of the spectrum as well as extending the photoconductivity to even longer wavelengths (up to 1100 nm) with a maximum at 690 nm (modulated illumination, curve *5*) or at 710 nm (steady illumination, curve *2*). The photosensitivity in the spectral region beyond 700 nm is higher with steady than with modulated illumination, showing that the contribution to $\Delta\sigma_{\sim}$ from slow processes is considerable in this region. The maximum of $\Delta\sigma_{\sim}$ coincides with the maximum of $\Delta\sigma_{=}$ of trigonal selenium crystals[88], and is shifted far into the long-wavelength region as compared with the $\Delta\sigma_{=}$ maximum of polycrystalline layers (630 nm).[25]

On lowering the temperature $\Delta\sigma_{\sim}$ is found to decrease, unlike $\Delta\sigma_{\sim}$ for layers with a low content of crystalline phase. The temperature dependence of $\Delta\sigma_{\sim}$ is described by the expression $\Delta\sigma_{\sim} = \Delta\sigma^{0} \exp(-\Delta E/kT)$, where the thermal activation energy $\Delta E = 0.03$ eV is the same for carriers photo-generated in the bulk ($\lambda = 600$ nm) or at the surface ($\lambda = 436$ nm) of the layer. The activation energy is needed, apparently, for the photo-carriers to overcome intermolecular (but not intercrystalline) energy barriers. In practice the displacement of the carriers at a frequency of 10^{10} Hz in a field of 10^{2} V cm^{-1} is less than 50 Å (the

carrier mobility in amorphous selenium is much less than 50 $cm^2 V^{-1} s^{-1}$). Thus the carrier displacement is much smaller than the size of the micro-crystals, which are usually several thousands of Ångstroms in diameter.

Many of the phenomena which we have discussed can be interpreted by the exciton model of photo-generation in selenium, as we shall show below. Here we only need to point out that the changes in the "structure–property" relationship observed at ultra-high frequency have provided a solution to the opposite problem: the use of photoconductivity at ultra-high frequency as a method of studying the degree of heterogeneity of glassy selenium[90].

IV. AMORPHOUS ANALOGUES OF SELENIUM CRYSTAL STRUCTURES

1. Structure

It may be assumed that if a molecular solid can exist in several crystalline modifications, with different types of short-range order, the solid should also exist in several amorphous structures with different types of short-range order (and therefore with different energy spectra). Among the possible examples of substances (or, indeed, elements) showing several amorphous structures selenium is a particularly good choice, because it can also exist in several crystalline modifications differing in molecular structure and therefore in short-range order.

Selenium layers prepared from a molecular vapour at a given temperature, at a given rate of condensation and substrate temperature, and homogenised under prescribed conditions, can form an amorphous state with two different amorphous structures (the amorphous forms of selenium) or consisting of a mixture of these two amorphous structures[7]. In contrast to the supercooled state, the short-range order in amorphous selenium manifests itself as a constant interatomic distance and also as an arrangement of atoms in definite configurations, leading to a diffraction pattern with several sharp maxima.

The first amorphous form of selenium is formed by evaporating the element from a melt at 220–270°C, condensing the vapour on a substrate at 18–40°C, and annealing the layer in a vacuum at room temperature for 30 h. This structure has a definite diffraction pattern. Its structural units are distorted structural units of the crystal lattice of the monoclinic α and β modifications: molecular rings consisting of eight atoms. During the formation of the structure these rings polymerise into agglomerates responsible for the "cobble-stone" outline of the sample surface.

The second amorphous form of selenium is formed by evaporation from a melt at a temperature above 350°C, condensation of the vapour on a substrate at 50–80°C, and subsequent annealing of the layers at 50°C in a vacuum for 20–30 min. This structure also gives a well defined diffraction pattern. The structural units of the second amorphous form are distorted structural units of the crystal lattice of trigonal selenium: short molecular chains. During the formation of the structure, the predominant process is polymerisation of the short molecular chains into long polymeric chains, randomly interweaved and looped.

The intermediate amorphous state of selenium is formed at moderate rates of evaporation on a substrate at 40–60°C, with slow cooling of the layer to room temperature. The diffraction pattern of this structure depends on the relative numbers of units of the first and of the second amorphous form. Using electron-diffraction results on the radii of the coordination spheres and on the coordination numbers, and making allowance for the presence of atomic selenium in the intermediate state, Nabitovich[7] concluded that the intermediate amorphous state includes not only ring and chain molecules of different size but also a significant number of selenium atoms, which tend to attach themselves to other atoms or to the ends of other molecules in a tetrahedral configuration. The first and the second amorphous form contain ~ 10% of these atoms, which join together the distorted ring or chain molecules and allow them to polymerise. Hence the main difference between the amorphous structures and the crystalline lattices is that the structural units in the former lack the parallel arrangement of the latter.

2. Photoelectric Phenomena in the Amorphous Analogues of the Selenium Crystal Structures

The first study[23] of the photoelectric properties of the amorphous analogues of selenium crystal structures aimed to explain the influence of short-range order on the photoelectric properties of various amorphous structures and to compare them with the properties of the corresponding crystalline structures. The measurements were made on layers of amorphous selenium with two types of molecular structure, prepared by vacuum evaporation of selenium of B_4 grade (99.9999% Se) with controlled melt and vapour temperature (230–250°C), deposition rate ($\leqslant 30$ Å s^{-1}), residual gas pressure (10^{-6} mmHg), and substrate temperature (20°C for the first type of structure, consisting mainly of ring molecules, and 55°C followed by vacuum annealing for the second type of structure, consisting mainly of chain molecules). Great care was taken to ensure the absence of crystalline phase in the layers. The structure of the surface of the layer, and of that of the sub-layer adjacent to the substrate, was investigated by the carbon replica method in an EM-5 electron microscope (20 000 × magnification). Fig. 3 shows some micrographs of amorphous selenium layers obtained by this method (*e*, *f*) and by scanning electron microscopy (*a*, *b*, *c*, *d*). The layer surface, the cross-section of the layer, and the substrate surface are clearly visible in the SEM pictures (*a*, *b*, *c*, *d*). With amorphous selenium films the surface of the layer and that of the sub-layer on the side of the substrate are smooth, specular, and free from microscopic inclusions of crystalline selenium, and the electron diffraction patterns (Fig. 3*g* and 3*h*) are typical of amorphous structures, with two or three diffuse rings (clearly visible in the microdensitometer traces of Fig. 3*j* and 3*k*). After heat treatment of these layers at 70°C microscopic inclusions of crystalline selenium appear in the amorphous selenium. These are clearly visible in the micrographs, and they are accompanied by the formation of spots on the diffraction pattern (Fig. 3*i*).

We should note that these methods of structural analysis can detect crystalline inclusions in the amorphous selenium layers only a few tens of Ångstroms in diameter. The reflection electron diffraction method is the most "non-destructive" method of studying amorphous selenium structures, and is therefore preferable to the simpler transmission method. By varying the thickness of the layers and by examining structurally both the free surface and the surface in contact with the substrate (after removing the layer from the substrate), and also by studying both surfaces and the cross-section of the layer with an electron

microscope, using shadowed carbon replicas, we have obtained reliable information on the amorphous forms of selenium[23,104] confirming the results of the leading workers on the amorphous selenium structures (Nabitovich, Richter, Herre, and others)[7,29,68].

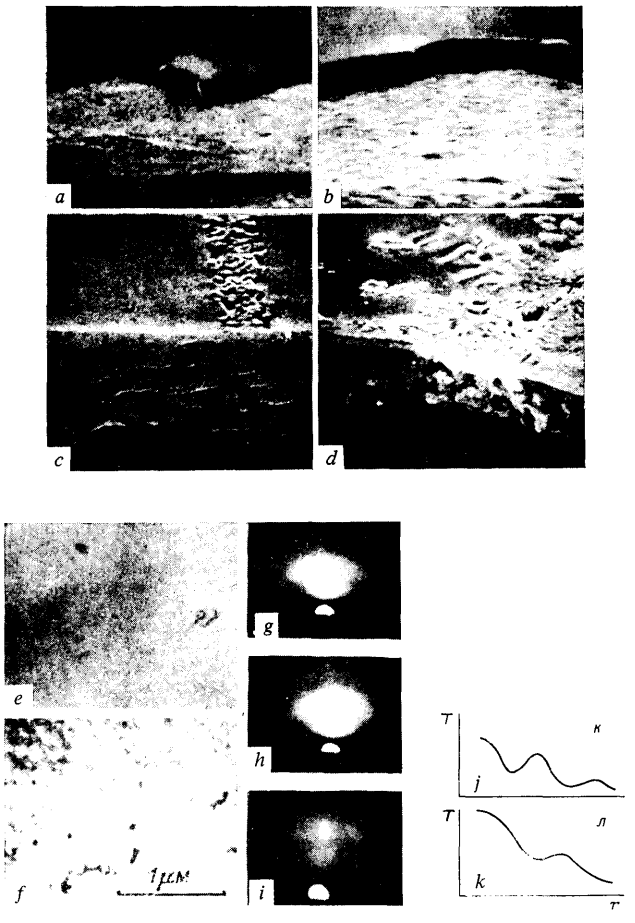


Figure 3. Electron diffraction patterns and micrographs of amorphous selenium structures[21,104]: *a*) and *e*) amorphous analogue of monoclinic selenium (free surface and substrate interface respectively), magnification × 14 000; *b*) and *f*) amorphous analogue of trigonal selenium; *c*) and *d*) for comparison, amorphous selenium containing some crystalline phase; *g*), *h*), and *i*) electron diffraction patterns for *a*), *b*), and *c*) respectively; *j*) and *k*) microdensitometer traces of the diffraction patterns of the amorphous analogues of monoclinic (*g*) and trigonal (*h*) selenium.

Studies of the spectral distribution of photoconductivity in strong electric fields (electrophotographic sensitivity), of photoconductivity at ultra-high frequency (10^{10} Hz), of the capacitive photo-e.m.f., and of the effect of light on the contact potential difference, made on the same samples over the spectral region 360–800 nm, have shown substantial differences in photoelectric properties between the two amorphous structures of selenium (Fig. 4). Firstly, the photo-effect spectra for selenium in one of the amorphous structures (curves *1*(*2*), *2*(*2*), *3*(*2*) of Fig. 4) show a marked shift towards the long wavelength region in comparison with the other amorphous structure (curves *1*(*1*), *2*(*1*), *3*(*1*), *4*(*1*) of Fig. 4). Secondly, the amorphous selenium structures have different photoconductivity types: one of the amorphous structures conducts mainly by positive holes, the other mainly by electrons. Thirdly, one of the amorphous structures has a fairly high photoconductivity at 10^{10} Hz (curve *2*(*2*) of Fig. 4).

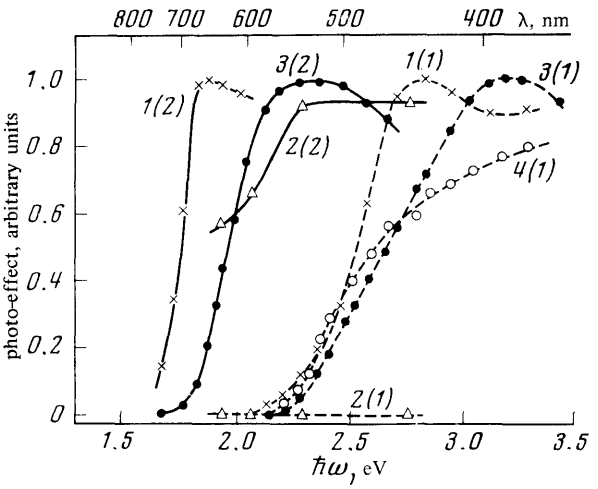


Figure 4. Isoenergetic spectra for the photo-effect in the amorphous analogues of the crystalline selenium structures[23]: *1*) d.c. photoconductivity (electrophotographic sensitivity), *2*) photoconductivity at 10^{10} Hz, *3*) photo-e.m.f., *4*) contact potential difference; in all curves (*1*) denotes the amorphous analogue of monoclinic selenium and (*2*) the amorphous analogue of trigonal selenium.

Comparison of the photo-properties of the amorphous and the crystalline structures has shown[23,92,104] that the two amorphous selenium structures with different short-range order are the amorphous analogues of the known crystalline structures of selenium (monoclinic and trigonal). The transition from crystal to amorphous analogue shows the theoretically predicted shift of the absorption edge towards longer wavelengths (Fig. 4).

The work described above has confirmed the crucial importance of short-range order in determining the properties of materials, and it has shown that short-range order in disordered materials can be controlled by varying the molecular structure: the survival of the molecular structure of molecular (polymeric) solids during the crystal–glass transition enables the glass to "remember" the short-range order (and the properties) of the crystal and to "forget" the long-range order.

To conclude this section we shall consider to what extent the photoelectric properties of amorphous selenium could be due to an undetected crystalline phase.

Existing methods of analysis by electron microscopy and electron diffraction methods, coupled with solid-state photoelectric spectroscopy, offer a fairly extensive and sensitive check on the phase composition and the molecular

state of selenium samples. As stated above, the following non-crystalline selenium structures (with different properties) have been recognised: amorphous (glassy) selenium, amorphous–crystalline selenium (amorphous selenium containing some crystalline phase), amorphous–crystalline selenium with a phase boundary (an amorphous layer with a crystalline sub-layer), and amorphous analogues of the crystalline selenium structures (monoclinic and trigonal). The role of the crystalline phase in the amorphous and amorphous–crystalline selenium structures has been discussed above. The existence of amorphous forms of selenium with structural units of crystalline selenium, demonstrated by Richter, Nabitovich, and others, is no longer in doubt. Recent work has shown[23] that the amorphous forms of selenium are true analogues of the corresponding crystalline structures, and that the crystal–glass transition in the appropriate pairs is accompanied by the theoretically predicted changes in optical and photoelectric properties.

Hence the properties of the amorphous analogues differ from those of amorphous selenium with crystalline inclusions or with a crystalline sub-layer in the following respects: the photoconductivity spectra at 10^{10} Hz, the spectra of the light-induced changes in contact potential difference and in capacitive photo-e.m.f., the photosensitivity spectra in the EP regime, the photoluminescence spectra (many lines in trigonal selenium[84] and a broad band in the amorphous analogue), the temperature dependence of the optical absorption edge[3], and the shape of the thermally stimulated conduction spectra[93].

V. PHOTOSENSITIVITY AND THE STRUCTURAL SENSITISATION OF THE PHOTO-EFFECT

Studies of non-photoactive absorption in molecular (polymeric) solids have led to the discovery of the phenomenon which we have termed structural sensitisation of the photo-effect[91]: a dependence of the spectral distribution and magnitude of the quantum yield for the internal photo-effect of molecular photoconductors upon the molecular and super-molecular structure of the solid. The phenomenon stems essentially from the photogeneration of current carriers in molecular photoconductors (in contrast to the photogeneration in classical semiconductors of the germanium and silicon type) through the state of a bound hole–electron pair (or exciton) over a wide spectral region. The features of the molecular and super-molecular structure determine the probability of generating free charge carriers from the bound state[28].

Let us consider in greater detail the photogeneration of free carriers in the amorphous analogues of the crystalline selenium structures. The theory of excitons in disordered semiconductors has been developed by Bonch-Bruevich[94] in recent years. We know at least three reasons for the lack of sharp absorption lines when excitons are present in disordered semiconductors. Firstly we have small-scale fluctuations in the electric field, which broaden the exciton lines; there is also strong scattering of the electrons, resulting in non-conservation of the quasi-momentum; lastly, the absorption coefficients are not additive, so that if an additional spectrally dependent absorption mechanism is present (in parallel with the exciton mechanism) the exciton structure of the absorption spectrum becomes blurred. However, the coulombic field must be acting on the electron and the hole as it does in crystals, and it must lead to the formation of bound states. Furthermore many disordered structures have relatively small dielectric constants, and if the effective mass of the carriers is not too small this should result in a large binding energy.

The presence of excitons had been previously suggested by various workers (Hartke, Regensburger, Siemsem, Fenten, Stuke, Davis, Boon) to account for various properties of amorphous selenium[84,95,96,100,101]. Our more recent investigation[92] differed from the earlier work on amorphous selenium in combining measurements of optical properties and of the quantum yield of the internal photo-effect as a function of quantum energy, temperature, and applied field on the same samples in order to reveal exciton effects. Layers of amorphous selenium were prepared by the molecular beam method in a vacuum[23] as analogues of monoclinic (first amorphous form, I AF) and trigonal (II AF) selenium, with different molecular structures (eight-membered rings and linear molecules up to several hundreds of atoms in length).[23] The thickness of the layers was varied between 0.1 and 10 μm. Tests for the absence of crystalline phases were made by electron microscopy and electron diffraction: this combination of methods could detect crystalline inclusions a few tens of Ångstroms in diameter within the amorphous layers. The quantum yield of the internal photo-effect (η) was measured in the electrophotographic regime; the low-field photoconductivity was measured with extremely small displacements of the charge carriers (a few Ångstroms) using a frequency of 10^{10} Hz with both steady and modulated illumination. The diffuse reflectance and the transparency of the layers were measured with and without an applied electric field of 2×10^5 V cm^{-1}; the kinetics of photo-discharge (in the EP regime) and of luminescence were studied at quantum energies in the range 1.5–3.3 eV and temperatures in the range 4.2–300 K, using SF-4 and SF-8 spectrophotometers and a cryostat designed to allow all the measurements to be done on the same sample.

The temperature shift of the absorption edge of the amorphous forms of selenium (Fig. 5*a* for I AF, curves *1* and *2* of Fig. 5*b* for II AF), unlike the temperature shift for crystalline selenium (curves *3* and *4* of Fig. 5*b*), depends on the quantum energy, falling to zero as the energy of the quantum increases[3]. The application of an electrostatic field of up to 2×10^5 V cm^{-1} shifts the absorption towards smaller quantum energies (Franz–Keldysh effect), but the change in transparency of the film due to this effect is less than 1%. Toyazawa's theory of localised excitons was used to analyse the temperature shift of the absorption edge. Transition probabilities for non-photoactive absorption, which can be compared with theory, were calculated by the method of Hartke and Regensburger[95], which is convenient for the case of several independent mechanisms of optical absorption. The experimentally determined transition probabilities $\epsilon_2^H \cdot (\hbar\omega)^2$, where ϵ_2^H is the imaginary part of the dielectric constant ϵ, corresponding to the non-photoactive absorption process (indicated points in curves *4–6*), agree quite well with theoretical predictions (solid curves *4–6* of Fig. 5*a*). The calculation is correct for the edge region of the non-photoactive absorption, for which the quantum yield of the internal photo-effect is $\eta \simeq 0$, and it explains the temperature dependence of the position of the absorption edge and its Urbach behaviour in terms of localised excitons.

When $\hbar\omega$ increases the excitons (of the Wannier–Mott type) dissociate in a strong field to give free charge carriers, and η becomes a function of quantum energy, electric field, and temperature. The η spectra (Fig. 6*a*)

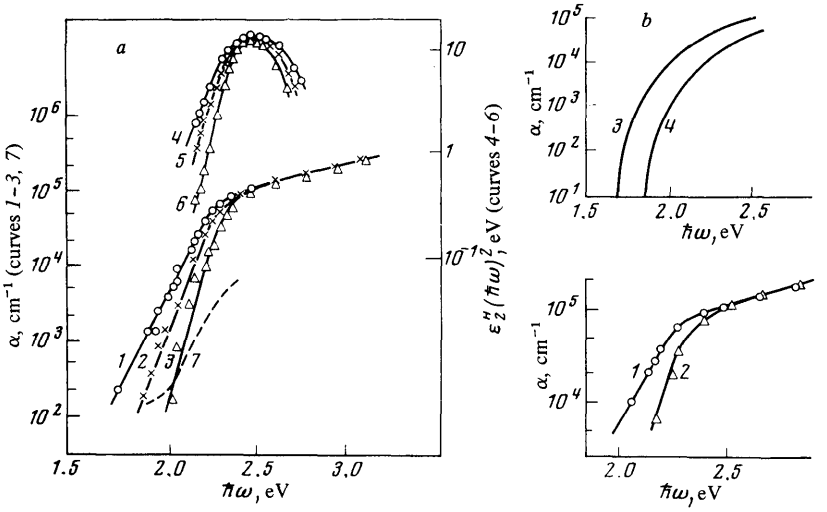


Figure 5. Optical properties of the amorphous analogues of crystalline selenium structures[103]: (*a*) absorption coefficient α of the amorphous analogue of monoclinic selenium: *1*) 300, *2*) 200, *3*) 95 K; *4*)–*6*) are the probabilities of the photoconducting transitions (*4*) 300, *5*) 200, *6*) 95 K, field 2×10^5 V cm^{-1}); *7*) absorption coefficient α of monoclinic selenium[24]; (*b*) absorption coefficient α of the amorphous analogue of trigonal selenium: *1*) 300, *2*) 95 K. The α values of trigonal selenium[109] are also shown for comparison: *3*) 300, *4*) 93 K.

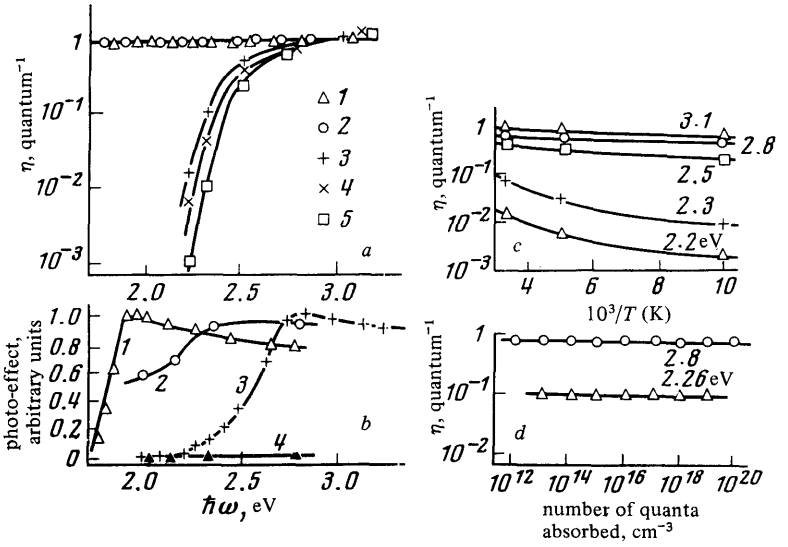


Figure 6. Quantum yield (*a*) of the internal photo-effect (*b*) and its temperature (*c*) and concentration (*d*) dependence[92]: (*a*) *1*) trigonal selenium and *2*) its amorphous analogue, field 2×10^5 V cm^{-1}, $T = 300$ K; *3*)–*5*) amorphous analogue of monoclinic selenium: *3*) 300, *4*) 200, *5*) 95 K, field 2×10^5 V cm^{-1}; (*b*) photo-effect in the highest possible (*1*, *3*) and in low (*2*, *4*) fields for the amorphous analogues of trigonal (*1*, *2*) and monoclinic (*3*, *4*) selenium; *c*) and *d*) refer to the amorphous analogue of monoclinic selenium.

and their dependence on temperature (Fig. 6*c*) and on field (Fig. 6*d*) are quite different for the two amorphous forms of selenium. For II AF (curve *1* of Fig. 6*a*), as for trigonal selenium (curve *2* of Fig. 6*a*), the η value is close to unity and practically constant in the region of 1.7–3.1 eV, i.e. up to the absorption edge, the carriers being generated in pairs. Conversely, for I AF (curves *3–5* of Fig. 6*a*) η decreases as the quantum energy, the temperature, and the field decrease, reaching zero at fields of the order of 10^2 V cm^{-1} (curve *4* of Fig. 6*b*), while the spectrum is shifted into the centre of the absorption band (the "red anomaly" according to Moss). Under these conditions, with a field of 2×10^5 V cm^{-1} and quantum energies between 2.8 and 2.26 eV, η is independent of the number of quanta absorbed over a range of eight orders of magnitude up to 10^{20} cm^{-3} (Fig. 6*d*), showing that concentration-dependent recombination is absent and that the carriers are generated in pairs.

The features observed for the I AF form of selenium, including carrier generation in pairs, independence of η upon ionisation density, increase of η with quantum energy, and variation of the activation energy of η (Fig. 6*c*) with quantum energy (falling to zero at the higher quantum energies), all suggest an exciton mechanism of photogeneration through the state of a coulombically bound pair. The results[92] are consistent with the theory of photogeneration in selenium developed by Pai[97,108], Ing[97], Tabak[98], Warter[98,99], Davis[100], and Vishchakas and Montrimas[102].

For the amorphous analogue of trigonal selenium we may again assume that carrier generation occurs through an exciton stage, but in this case the excitons are effectively dissociated by a small electric field in accordance with the theory of Bonch-Bruevich. In this model the quantum yield should not be lowered substantially by a decrease in the applied field: as shown in curve *2* of Fig. 6*b*, the quantum yield does not fall to zero (in contrast to the case of the analogue of monoclinic selenium).

Both amorphous structures give luminescence bands at 4.2 K, but the luminescence is quenched by increase of temperature[103]: in both cases the width of the band is 0.23 eV. However the position of the band relative to the forbidden gap E_{opt} and the spectral distribution of the luminescence yield are very different in the two cases. For I AF (Fig. 7*a*) the quantum energy corresponding to the peak of the luminescence band is 1.80 eV, and E_{opt} = 1.88 eV[104] (see Table); the quantum yield of the luminescence φ_{lum} depends on the energy of the quantum, falling to zero as the quantum increases, as well as varying in a sense opposite to that of η. We must stress three facts. Firstly, at low values of $\hbar\omega$ and at low fields $\eta \simeq 0$, and $\varphi_{lum} = 0$, showing that the luminescence arises from annihilation of bound pairs rather than from recombination of free carriers. Secondly, increasing $\hbar\omega$ leads to $\eta \simeq 1$, but in this case $\varphi_{lum} = 0$, i.e. the free carriers do not contribute to the luminescence. Lastly, the changes in opposite sense of the η and φ spectra follow unambiguously from the alternative mechanisms: annihilation of the exciton, with luminescence, or dissociation with formation of free current carriers.

Optical and photoelectric forbidden gap (E) of selenium with different molecular structures.

E, eV	Eight-membered ring		Polymeric chain	
	crystal	glass	crystal	glass
E_{phot}	2.48	2.53	1.78	1.79
E_{opt}	2.0	1.88	1.78	1.81

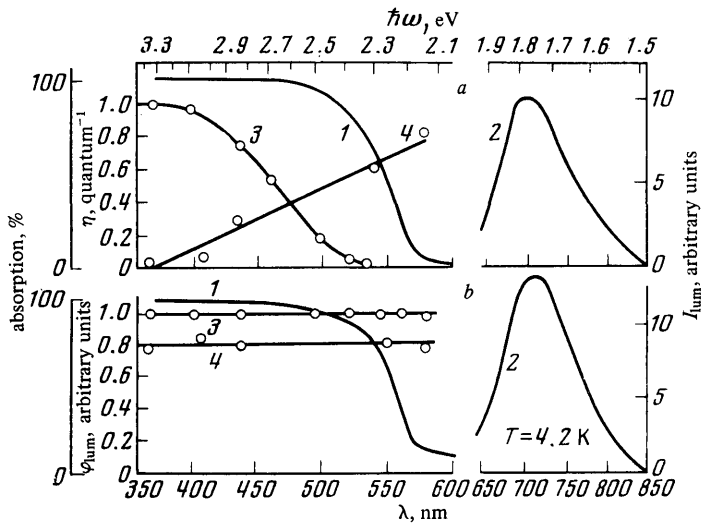


Figure 7. Spectra of the photo-processes in the amorphous analogues of the crystalline selenium structures (*a*) monoclinic, *b*) trigonal)[103]: *1*) absorption, *2*) photoluminescence (I), *3*) quantum yield of the internal photo-effect η (extrapolated from 30 K), *4*) quantum yield of the photoluminescence φ.

The observed luminescence cannot be due to impurities, which could not explain the specific effects discussed above, and would also be inconsistent with the fact that Urbach's rule is found to apply up to absorption coefficients greater than 10^4 cm^{-1}.[96] However participation of impurities or defects in the luminescence of amorphous selenium is possible in principle, but only if we retain the assumption of interaction via excitons: in this way the luminescence can be interpreted as exciton luminescence. The ground state of the exciton, measured[92] from the luminescence spectrum (E_{exc} = 1.80 eV), lies 0.08 eV below the bottom of the conduction band (E_{opt} = 1.88 eV). We note that E_{opt} was determined according to Sturge's criterion for α, corresponding to the mobility threshold ($\sim 10^3$ cm^{-1}), whereas E_{phot} was determined by the Moss criterion[104]. The photon energy corresponding to E_{exc} according to Toyazawa's theory and measured from the photoconductivity spectrum was 2.44 eV,[3] i.e. 0.09 eV lower than E_{phot} = 2.53 eV. It may be assumed that the difference between the E_{exc} values measured in absorption and in emission is due to energy dissipation by the excited pair.

In amorphous selenium with a molecular chain structure the quantum energy at the luminescence maximum (1.75 eV) is close to E_{opt} = 1.78 eV, and the φ_{lum} spectrum is correlated to the η spectrum and does not depend on $\hbar\omega$. This behaviour, and also the very high quantum yield η of unity, allow us to interpret the luminescence as recombination-induced, of a type previously observed in amorphous chalcogenide semiconductors[105-107]. As Fig. 7 shows, no exciton absorption peak is observed in either amorphous structure at temperatures down to 4.2 K.

---o0o---

The optical and photoelectric properties of amorphous selenium structures discussed above indicate the existence of exciton effects in disordered polymeric semiconductors.

By comparing the roles of exciton effects in the photogeneration of charge carriers in organic and in inorganic polymeric photoconductors[28] we conclude that these effects are weaker in inorganic photoconductors because the coulombic interaction of the hole–electron pair created by the absorption of a light quantum is more effectively screened in these materials.

REFERENCES

1. S.G. Grenishin and Yu.A. Cherkasov, Fiz. Tverdogo Tela, 6, 2831 (1964).
2. S.G. Grenishin, Yu.A. Cherkasov, L.N. Vinokurova, N.B. Zakharova, and A.I. Myl'nikova, Symposium, "Mezhdunarodnyi Kongress po Fotograficheskoi Nauke" (International Congress on Photographic Science), Izd. Nauka, Moscow, 1970, Section E, p. 240.
3. Yu.A. Cherkasov and L.G. Kreitor, Fiz. Tverdogo Tela, 16, 2407 (1974).
4. Yu.A. Cherkasov, Symposium "Mezhdunarodnyi Kongress po Fotograficheskoi Nauke" (International Congress on Photographic Science), Dresden, 1974, Vol. 2, p. 63.
5. S.G. Grenishin, Yu.A. Cherkasov, L.G. Kreitor, M.I. Cherkashin, and M.G. Chauser, "Pervaya Vsesoyuznaya Konferentsiya po Besserebryanym i Neobychnym Fotograficheskim Protsessam" (First All-Union Conference on Silverless and Unconventional Photographic Processes), Kiev, 1972, p. 41.
6. D.M. Chizhikov and V.P. Schastlivyi, "Selen i Selenidy" (Selenium and Selenides), Izd. Nauka, Moscow, 1964.
7. I.D. Nabitovich, Thesis, L'vov, 1970.
8. I.D. Nabitovich, Ya.I. Stetsiv, and Ya.V. Voloshchuk, Zhur. Nauch. Prikl. Fotogr. Kinematogr., 11, 27 (1966).
9. N.B. Hannay (Editor), "Semiconductors" (Translated into Russian), Moscow, 1962, p. 371.
10. K.E. Kirk, "Encyclopaedia of Chemical Technology", Vol. 2, New York, 1954, p. 145.
11. E. Mooser and W.B. Pearson, J. Phys. Chem. Solids, 7, 65 (1958).
12. "Gmelin's Handbuch der anorganischen Chemie", 8 Aufl. System-Nummer 10, Selen, 1942.
13. A. von Hippel, J. Chem. Phys., 16, 372 (1948).
14. "Gmelin's Handbuch der anorganischen Chemie", 8 Aufl. System-Nummer 10, Selen, 1952.
15. A.I. Andrievskii, I.D. Nabitovich, and Ya.I. Stetsiv, Symposium "Elektrofotografiya i Magnitografiya" (Electrophotography and Magnetography), Izd. Mintis, Vil'nyus, 1972, p. 91.
16. R.D. Burbank, Acta Cryst., 4, 140 (1951).
17. R.D. Burbank, Acta Cryst., 5, 236 (1952).
18. R.E. Marsh, L. Pauling, and J.D. McCullough, Acta Cryst., 6, 71 (1953).
19. B.A. Kotov, N.M. Okuneva, A.R. Regel', and A.L. Shakh-Budagov, Fiz. Tverdogo Tela, 9, 1227 (1967).
20. A. Eisenberg and A.V. Tobolsky, J. Polymer Sci., 96, 19 (1960).
21. N.B. Zakharova and Yu.A. Cherkasov, Symposium "Fizicheskie Osnovy Elektrofotografii" (Physical Foundations of Electrophotography), Izd. Mintis, Vil'nyus, 1969, p. 177.
22. Yu.A. Cherkasov and L.N. Ionov, Fiz. Tverdogo Tela, 9, 630 (1967).
23. N.B. Zakharova and Yu.A. Cherkasov, Fiz. Tverdogo Tela, 12, 7, 1977 (1970).
24. Yu.G. Asadov and M.Ya. Bakirov, Izv. Akad. Nauk SSSR, Ser. Neorg. Mater., 5, 459 (1969).
25. M.A. Gilleo, J. Chem. Phys., 19, 1291 (1951).
26. T.O. Tuomi, Phys. Status Solidi, 28, 329 (1968).
27. A.M. Meshkov and I.A. Akimov, Dokl. Akad. Nauk SSSR, 162, 306 (1965).
28. Yu.A. Cherkasov, Izv. Vys. Ucheb. Zaved., Fiz., No. 2, 86 (1976).
29. H. Richter and F. Herre, Z. Naturforsch., 13-A, 874 (1958).
30. H. Krebs and Y. Schultze-Gebhardt, Acta Cryst., 8, 412 (1955).
31. A.R. Regel', "Stroenie i Fizicheskie Svoistva Veshchestva v Zhidkom Sostoyanii" (Structure and Physical Properties of Matter in the Liquid State), Izd. Kiev. Univ., Kiev, 1954, p. 117.
32. H. Richter and F. Herre, Naturwissenschaft., 44, 31 (1957).
33. V.M. Glazov, S.N. Chizhevskaya, and N.N. Glagoleva, "Zhidkie Poluprovodniki" (Liquid Semiconductors), Izd. Nauka, Moscow, 1967.
34. I.N. Stranski, R. Kraischew, and H. Krastanow, Z. Krist., 88, 325 (1934).
35. V.I. Blum and A.R. Regel', Zhur. Tekh. Fiz., 23, 964 (1953).
36. M.V. Reznik and M.I. Korsunskii, Izv. Vys. Ucheb. Zaved., Fiz., No. 3, 107 (1960).

37. A. I. Andrievskii, I. D. Nabitovich, and P. I. Kripyakevich, Dokl. Akad. Nauk SSSR, 124, 321 (1959).
38. A. I. Andrievskii and I. D. Nabitovich, Nauch. Zap. L'vov, Politekh. Inst., 58, 82 (1958).
39. H. Krebs and W. Morsch, Z. anorg. Chem., 263, 305 (1950).
40. R. C. Keezer and M. W. Bailey, Materials Res. Bull., 2, 185 (1967).
41. H. Krebs and W. Morsch, Z. anorg. Chem., 263, 305 (1950).
42. G. Busch and O. Vogt, Phys. Acta, 30, 224 (1962).
43. L. Graham and R. Chang, J. Appl. Phys., 36, 2983 (1965).
44. R. C. Keezer and M. W. Bally, Materials Res. Bull., 2, 185 (1967).
45. L. Holland, "Vacuum Deposition of Thin Films" (Translated into Russian), Gosenergoizdat, Leningrad, 1963.
46. V. V. Artamonova and N. M. Gal'vidus, Obmen Opytom v Radioelektronnoi Prom., 7, 22 (1966).
47. M. B. Jajna, I. M. Toguri, and I. E. Dutrizae, Canad. J. Phys., 46, 447 (1968).
48. A. N. Nesmeyanov, "Davlenie Parov Khimicheskikh Elementov" (Vapour Pressure of the Elements), Izd. Akad. Nauk SSSR, Moscow, 1961, p. 281.
49. K. Niwa and I. Sibata, J. Fac. Sci. Univ., Tokyo, 3, 75 (1940).
50. V. V. Illarionov and L. M. Lapina, Dokl. Akad. Nauk SSSR, 114, 1021 (1957).
51. D. M. Yukhtanov, "Proizvodstvo Selena i Tellura" (Production of Selenium and Tellurium), Metallurgizdat, Moscow, 1955.
52. A. A. Kudryavtsev, "Khimiya i Tekhnologiya Selena i Tellura" (Chemistry and Technology of Selenium and Tellurium), Izd. Vysshaya Shkola, Moscow, 1961.
53. P. P. Barzdain and N. V. Alekseev, Zhur. Strukturnoi Khim., 9, 520 (1968).
54. L. G. Vinokurov, V. A. Islyamov, and P. M. Podvigalkin, Zhur. Nauch. Prikl. Fotogr. Kinematogr., 11, 201 (1966).
55. H. Levinsten, J. Appl. Phys., 20, 306 (1949).
56. R. Brehler, Z. Physik, 212, 212 (1968).
57. I. D. Nabitovich, Ya. V. Voloshchuk, and Ya. I. Stetsiv, Zhur. Nauch. Prikl. Fotogr. Kinematogr., 11, 95 (1966).
58. H. Grimminger, H. Grüninger, and H. Richter, Naturwiss., 42, 256 (1955).
59. P. Keck, J. Opt. Soc. Amer., 41, 53 (1951).
60. S. A. Tauraitene and A. S. Tauraitis, "Voprosy Radioelektroniki" (Problems in Radio-electronics), Series 12, No. 25, 1964, p. 21.
61. H. Richter, Z. Naturforsch., 13A, 32 (1958).
62. V. P. Baltrushaitene and E. A. Montrimas, "Voprosy Radioelektroniki" (Problems in Radio-electronics), Series 12, No. 25, 1964, p. 17.
63. A. I. Andrievskii, I. D. Nabitovich, and Ya. V. Voloshchuk, Kristallografiya, 5, 369 (1960).
64. S. A. Semiletov, Trudy Inst. Kristallografii Akad. Nauk SSSR, 11, 115 (1955).
65. S. A. Semiletov, Kristallografiya, 4, 629 (1959).
66. A. I. Andrievskii, I. D. Nabitovich, Ya. I. Stetsiv, and Ya. V. Voloshchuk, Ukrain. Fiz. Zhur., 13, 1596 (1968).
67. E. H. Henninger and R. C. Buschert, J. Chem. Phys., 46, 586 (1967).
68. H. Richter, J. Non-Cryst. Solids, 8, 388 (1972).
69. R. Kaplow, T. A. Rowe, and B. L. Averbach, Phys. Rev., 168, 1068 (1968).
70. D. N. Nasledov, V. A. Dorin, and I. M. Dikina, Zhur. Tekh. Fiz., 25, 29 (1955).
71. I. D. Nabitovich, Ya. V. Voloshchuk, and Ya. I. Stetsiv, Zhur. Nauch. Prikl. Fotogr. Kinematogr., 11, 95 (1966).
72. V. G. Boitsov and B. A. Tazenkov, Optiko-mekhan. Prom., 5, 35 (1965).
73. G. N. Sandalov and B. A. Tazenkov, Uch. Zap. L'vov. Politekh. Inst., 384 (1), 145 (1968).
74. B. A. Tazenkov, V. G. Boitsov, G. N. Sandalov, I. B. Shneidman, L. N. Perenechaev, V. V. Branitskii, and P. V. Khaikin, Symposium "Elektrofotografiya i Magnitografiya" (Electrophotography and Magnetography), Izd. Mintis, Vil'nyus, 1972, p. 627.
75. B. A. Tazenkov, G. N. Sandalov, and I. B. Shneidman, "Pervaya Vsesoyuznaya Konferentsiya po Besserebryanym i Neobychnym Fotograficheskim Protsessam" (First All-Union Conference on Silverless and Unconventional Photographic Processes), Kiev, 1972, p. 69.
76. B. A. Tazenkov, V. G. Boitsov, G. N. Sandalov, and I. B. Shneidman, "Protsessy i Apparaty Elektrofotografii" (Electrophotographic Processes and Apparatus), Izd. Mashinostroenie, Leningrad, 1972.
77. Yu. K. Vishchakas, N. M. Gal'vidus, A. Yu. Matulenis, and S. A. Tauraitene, Symposium "Selen, Tellur, i Ikh Primenenie" (Selenium, Tellurium, and Their Applications), Izd. Akad. Nauk AzerbSSR, Baku, 1965, p. 143.
78. A. Yu. Matulenis, Yu. K. Vishchakas, G. V. Yushka, and N. M. Gal'vidus, Symposium "Selen, Tellur, i Ikh Primenenie" (Selenium, Tellurium, and Their Applications), Izd. Akad. Nauk AzerbSSR, Baku, 1965, p. 149.
79. E. A. Montrimas and B. M. Petretis, Symposium "Sostoyanie i Puti Povysheniya Kachestva Elektrofotograficheskoi i Kopiroval'no-mnozhitel'noi Tekhniki" (Present State of and Possible Improvements in Electrophotographic and Photocopying Techniques), Izd. Mintis, Vil'nyus, 1972, p. 31.
80. E. Montrimas and B. Petretis, Phys. Status Solidi (*a*), 15, 361 (1973).
81. A. A. Shatas, Thesis Abstracts, Vil'nyus, 1972.
82. V. G. Boitsov, G. A. Sukonkin, and B. A. Tazenkov, "Dvadtsatchetvertye Gertsenovskie Chteniya" (Twenty-fourth Gertsen Lectures), Izd. L'vov. Politekh. Inst. imeni Gertsena, L'vov, 1971, p. 89.
83. V. G. Boitsov, G. A. Sukonkin, and B. A. Tazenkov, "Pervaya Vsesoyuznaya Konferentsiya po Besserebryanym in Neobychnym Fotograficheskim Protsessam" (First All-Union Conference on Silverless and Unconventional Photographic Processes), Kiev, 1972, p. 65.
84. G. Weiser and I. Stuke, Phys. Status Solidi, 35, 747 (1969).
85. E. M. Trukhan, Pribory i Tekh. Eksper., No. 4, 198 (1965).
86. E. V. Batanov and I. A. Akimov, Dokl. Akad. Nauk SSSR, 154, 184 (1964).
87. S. G. Grenishin and Yu. A. Cherkasov, Zhur. Nauch. Prikl. Fotogr. Kinematogr., 7, 121 (1962).
88. B. Gudden and R. Pohl, Z. Physik, 35, 243 (1926).
89. W. E. Spear, Proc. Phys. Soc., 76, 816 (1960).
90. Yu. E. Gordienko, Thesis Abstracts, Khar'kov, 1969.

91. Yu. A. Cherkasov, Thesis Abstracts, Leningrad, 1975.
92. Yu. A. Cherkasov, Symposium "Struktura i Svoistva Nekristallicheskikh Poluprovodnikov" (Structure and Properties of Non-crystalline Semiconductors), (B. T. Kolomiets, Editor), Izd. Nauka, Leningrad, 1976, p. 282.
93. Yu. A. Cherkasov and I. Yu. Yurkan, Fiz. i Tekh. Poluprovodnikov, 7, 1008 (1968).
94. V. L. Bonch-Brujevitch and V. D. Iskra, Phys. Status Solidi (*b*), 68, 369 (1975).
95. I. L. Hartke and P. I. Regensburger, Phys. Rev., 139, 970 (1965).
96. K. I. Siemsem and E. W. Fenten, Phys. Rev., 161, 632 (1967).
97. D. M. Pai and S. W. Ing, Phys. Rev., 173, 729 (1968).
98. M. D. Tabak and P. I. Warter, Phys. Rev., 173, 899 (1968).
99. P. I. Warter, Appl. Opt. Suppl., 3, 65 (1969).
100. E. A. Davis, J. Non-Cryst. Solids, 4, 107 (1970).
101. M. R. Boon, J. Non-Cryst. Solids, 2, 177 (1971).
102. E. M. Montrimas and I. Vishchakas, "Second International Conference on Electrophotography", Washington, 1973, p. 220.
103. Yu. A. Cherkasov, Fiz. Tverdogo Tela, 16, 3690 (1974).
104. Yu. A. Cherkasov, Symposium "Opticheskie i Spektral'nye Svoistva Stekol. Tezisy Dokladov Tretego Vsesoyuznogo Simpoziuma 24–25 Okt. 1974" (Abstracts of Papers Presented to the Third All-Union Symposium on the Optical and Spectral Properties of Glasses, 24–25 October 1974), Leningrad, 1974, p. 5.
105. B. T. Kolomiets, T. N. Mamontova, E. A. Smotgonskay, and A. A. Babajev, Phys. Status Solidi (*a*), 11, 441 (1972).
106. B. T. Kolomiets, T. N. Mamontova, and A. A. Babajev, J. Non-Cryst. Solids, 4, 289 (1970).
107. B. T. Kolomiets and V. M. Lyubin, Phys. Status Solidi (*a*) 17, 11 (1973).
108. D. M. Pai and R. C. Enck, Phys. Rev., B11, 5163 (1975).
109. L. Müller, Studii si Cercetari Fiz. (Acad. RPR), 21, 1001 (1969).